Improved modelling and inversion of surface wave method

Chih-Ping Lin[1,2#], *Tsai-Jung* Wu[1], *Quoc Kinh* Tran[1] and Ernian Pan[1,2]

[1] *Disaster Prevention and Water Environment Research Center, National Yang Ming Chiao Tung University, 1001 Daxue Rd., Hsinchu 300, Taiwan*
[2] *Department of Civil Engineering, National Yang Ming Chiao Tung University, 1001 Daxue Rd., Hsinchu 300*
[#]*cplin.ce@nycu.edu.tw*

ABSTRACT

The multi-channel analysis of surface waves (MASW) is a widely employed surface wave method. The fundamental mode inversion is the usual scheme in MASW, because separating the fundamental mode from other high modes is feasible with an adequately long array. However, the extracted fundamental mode represents only part of the dynamic characteristics, it may deviate from the theoretical fundamental mode due to truncation effect, and part of it may correspond to another higher mode or leaky mode, resulting in mode misidentification. Conversely, the spectral analysis of surface waves (SASW) method features a more rigorous inversion scheme by matching the effective mode, but it may suffer from the tricky phase-unwrapping in the dispersion data reduction. This study introduces an improved dynamic response solution for elastic-layered media subjected to vertical loads. The proposed dynamic response solution is fast and accurate, facilitating the full wavefield inversion in terms of the frequency-velocity spectrum. The MASW frequency-velocity spectrum inversion considers testing configuration and comprehensively models all wave phenomena, including near-field effect, truncation effect, and leaky waves. The MASW frequency-velocity spectrum inversion merges the convenience of MASW dispersion analysis with the rigorous inversion scheme adopted by SASW. The new MASW frequency-velocity spectrum inversion is compared with the SASW effective mode inversion and MASW fundamental mode inversion. The results show that both SASW effective mode inversion and MASW frequency-velocity spectrum inversion produce better inverted results than the MASW fundamental mode inversion, while the process of MASW frequency-velocity spectrum inversion is more convenient and robust. Finally, a field example is used to demonstrate the applicability of frequency-velocity spectrum inversion.

Keywords: MASW; layered-system; dynamic response; full wavefield inversion

1. Introduction

Surface wave methods are fast, reliable, and widely used methods in geotechnical engineering, they are commonly adopted to infer the shear wave velocity (V_S) profiles in the field. Many types of surface wave methods are developed for near surface site characterization. These methods can be generally divided into two groups based on the data acquisition and corresponding dispersion analysis: the two-station method (spectral analysis of surface waves, SASW; Stokoe et al., 1994) and the multi-station method (multi-station analysis of surface waves, MASW; Park et al., 1999).

SASW is typically conducted by inducing a vertical impact on the ground surface and recording the signals at two stations, and the phase difference between the two receivers can be computed by Fourier transform. The apparent phase velocity between two receivers is then measured by the calculation of receiver spacing and phase difference. This apparent dispersion curve (i.e., the dominated phase velocity at each frequency) from two-station phase shift is "apparent" (or effective) because multiple modes including non-Rayleigh waves may be involved at the same time, and different receiver spacing is typically used to extend the effective frequency range of measurements. The SASW method requires a suitable inversion kernel capable of considering the effective mode, particularly when higher modes or non-Rayleigh waves are present. An important feature of SASW effective mode inversion is to consider of the actual configuration (the relation between source and receivers) and dynamic response.

On the other hand, MASW method samples the wavefield at multiple locations, allowing the identification of different modes through wavefield transformation. The dispersion relation can be determined through different methods, which could be divided into phase-based and transform-based methods. In transform-based methods, experimental data undergo transformation from the time-space domain to another domain, e.g., the frequency-velocity transform achieved via the phase shift method (Park et al., 1998). Wavefield transformation based on multi-station data avoids the tricky phase-unwrapping in data processing of SASW and provides visualization of separate dominant modes. When the receiver array is sufficiently long, current practice considers that the fundamental mode can be extracted from other possible higher modes. Hence, the fundamental mode inversion of MASW data is a common practice. However, the MASW-measured dispersion curves only use a piece of wavefield information, it may deviate from the normal modes due to the truncation effect and some dominant modes may not correspond to any of the normal modes (Lin et al., 2023).

A few studies seek an alternative approach that combines the convenient multi-channel data analysis and dynamic response calculation, performing the inversion by fitting the measured data in transformed domain, e.g., frequency-slowness domain and frequency-velocity domain (Forbriger, 2003; Ryden and Park, 2006; Dou and Ajo-Franklin, 2014). The full wavefield inversions in the transformed domain in these studies achieved better performance, but did not gain popularity, probably due to the high computational cost.

Based on the new fast algorithm in the frequency domain (Lin et al., 2022), a more rigorous inversion scheme, the inversion of full frequency-velocity spectrum from multi-channel data analysis, is proposed. The inverted results of the proposed approach are compared with two practical approaches, SASW effective mode inversion and MASW fundamental mode inversion. A field example will be used to demonstrate the feasibility of the proposed approach.

2. Full wavefield computation of vertical loading

2.1. Steady-state response

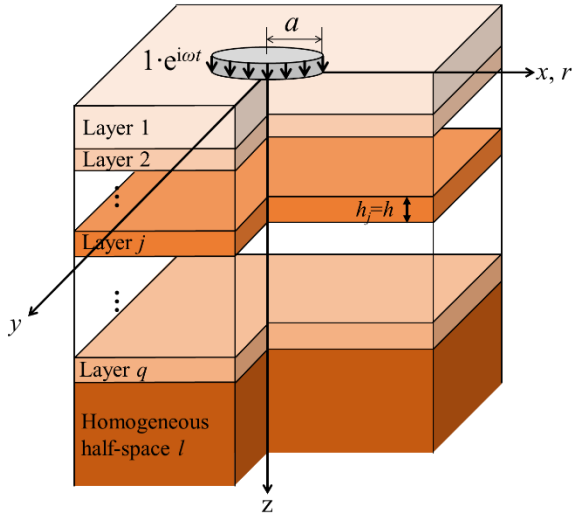

Figure 1. Schematic of the layered model subjected to circular loading.

For a multi-layered half-space subjected to a unit vertical load on the ground surface (Fig. 1), the vertical displacement fields on the ground surface as a function of time (t) and radius (r) is denoted as $w(t, r)$. Taking Fourier transform with respect to t and Hankel transform (Fourier-Bessel transform) with respect to space (i.e., r), and taking advantage of the axial symmetric condition, general solutions in the transformed domain, $\hat{w}(\omega,k)$, can be simplified and solved (Lin et al., 2022). The global stiffness matrix method (Kausel and Roësset, 1981) is adopted to address the layered system in the study for its simplicity and numerical stability. The global stiffness matrix [$\boldsymbol{K}$] links the nodal displacements and nodal forces, and the nodal displacements can then be solved. The steady-state frequency response (i.e., the response to time-harmonic loading) is the inverse Hankel transform of the solution:

$$W(\omega,r)=\int_{-\infty}^{\infty}\hat{w}(\omega,k)\hat{S}(k)J_0(kr)kdk \quad (1)$$

where ω is angular frequency ($\omega=2\pi f$, f is frequency), k is wavenumber. J_0 is the Bessel functions of the first kind of orders 0, and $\hat{S}(k)$ is the Hankel transform of the spatial variation of the load.

For efficient numerical computation, the Hankel transform can be replaced by the Fourier-Bessel series. Therefore, the continuous wavenumber in the wavefield becomes discrete k_m, with k_m being determined by the maximum radius (R) and discrete point number (M) in the space domain. As a result, the time-consuming numerical integration of the inverse Hankel transform can be replaced by Fourier-Bessel series expansion:

$$W(\omega,r)=\sum_m \hat{w}(\omega,k_m)\hat{S}(k_m)J_0(k_m r) \quad (2)$$

This dynamic response of an isotropic elastic layered half-space subjected to vertical loading was implemented and thoroughly validated in Lin et al. (2022). The proposed algorithm preserves the complete wavefield, including the near-field effect and leaky waves, and it is at least two-orders faster than the conventional integration transformation method, facilitating the full wavefield inversion in terms of the frequency-velocity spectrum.

2.2. Synthetic data of various V_S profiles

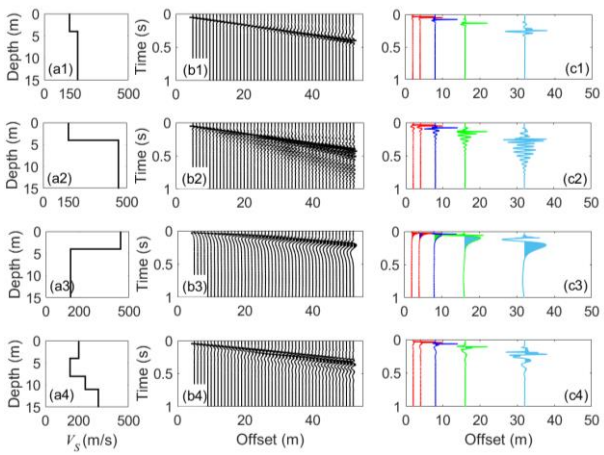

Figure 2. (a) Four different V_S profiles are used for generating synthetic time-domain data for (b) MASW and (c) SASW. Poisson's ratio and density are fixed at 1/3 and 2000 kg/m^3, respectively.

A few synthetic models for dynamic response simulation are set to examine the performance of different inversion approaches, so that the theoretical ground truth is known for benchmarking. Figure 2(a) shows four different models (denoted as Models 1 to 4) for generating synthetic time-domain data (waveforms). The Poisson's ratio and density are fixed at 1/3 and 2000 kg/m^3, respectively. These simplified synthetic models are selected to represent different dispersion scenarios. Model 1 is a two-layer model with mild V_S contrast, as a case in which the effective dispersion curve is mainly dominated by the fundamental mode. Model 2 is a two-layer model with high V_S contrast, which is a typical scenario for sites with shallow bedrock. Model 3 is a profile that the V_S in the underlying half-space is smaller

than the upper layer(s), which is similar to a pavement profile. Model 4 is a case with an embedded soft layer, which is a typical site condition where the surface layer is stiffer due to capillarity, desiccation, or surface compaction.

With the forward kernel proposed previously and Fourier series expansion, synthetic transient response (i.e., time-domain data) can be generated for different V_S profiles:

$$w(t,r) = \sum_n W(\omega_n, r)\hat{F}(\omega_n)e^{i\omega_n t} \quad (3)$$

where ω_n is determined by the maximum time window (T) and discrete point number (N) in the time domain; $\hat{F}(\omega_n)$ is the Fourier series of time variation of the load. The source wavelet is a half-sine function with 0.01 s duration. These time domain signals are taken as measured data in MASW and SASW data acquisition (Figs. 2(b) and (c)). Data with different receiver spacing (D=2, 4, 8 and 16 m) are generated for SASW; and the configuration with nearest offset (x_0) 5 m, receiver spacing (dx) 1 m, and survey length (L) 47 m is used for 48-channel MASW. This study investigated the full wavefield inversion based on the frequency-velocity spectrum, which is computed by the f-k transform (Gabriels et al., 1987) followed by converting the wavenumber (k) to phase velocity (v) as

$$\hat{W}(f,v) = \sum_m W(f, r_m)e^{i\frac{2\pi f}{v}r_m} \quad (4)$$

where $W(f, r_m)$ is the Fourier transform of the ground motion data, $w(t_n, r_m)$, in which t_n and r_m are the sampled times and receiver locations, respectively. The amplitude plot of the $\hat{W}(f,v)$ is further normalized by the maximum amplitude at each frequency to eliminate the source effect, and this normalized amplitude plot in f-v domain is referred to as the frequency-velocity spectrum in this study.

3. Inversion

3.1. Model parameterization and initial model

Parameterization is the first step in the inversion process, it includes deciding the depth to lower half-space (z_{max}) and layer number. The inversion is highly nonlinear when both V_S and layer thickness are considered in the inversion; as a result, a practical scheme, dividing the profile into several layers and inverting only for V_S, is adopted. In order to simplify the comparison, z_{max} is given as the actual depth in this study. Layer number (including half-space) is examined from 2 to 10 layers, where the thickness of each layer is decided by the ratio of z_{max} shown in Fig. 3, and the V_S profile is inverted accordingly. The simplest model that fits the data reasonably well will be taken as the inverted results to avoid over interpretation.

The initial model for inversion is estimated by the simplified inversion method that directly converts the apparent dispersion curve to V_S profile (Pelekis and Athanasopoulos, 2011). The apparent dispersion curve in the frequency-velocity spectrum (Fig. 4(a)) is first transformed into wavelength (λ) and phase velocity (v) domain (Fig. 4(b)). Then, it is further transformed into apparent depth (z_{app}) and apparent shear wave velocity ($V_{S,app}$) by converting the λ to apparent depth, z_{app}=0.5λ, and taking the apparent shear wave velocity as $V_{S,app}$=v/0.9 (Fig. 4(c)). An example of initial model for 7-layer inversion of Model 4 is shown in Fig. 4(c).

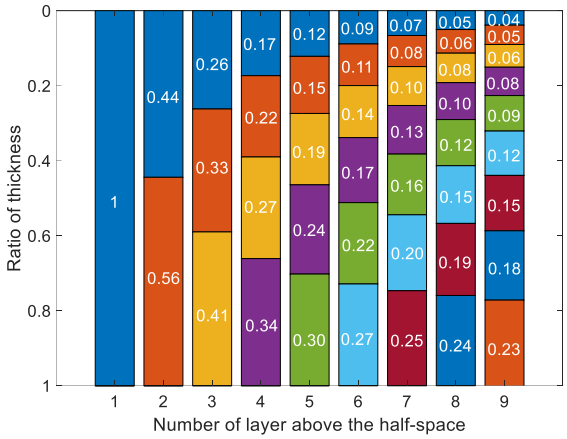

Figure 3. Schematic diagram of layer number and relative thickness.

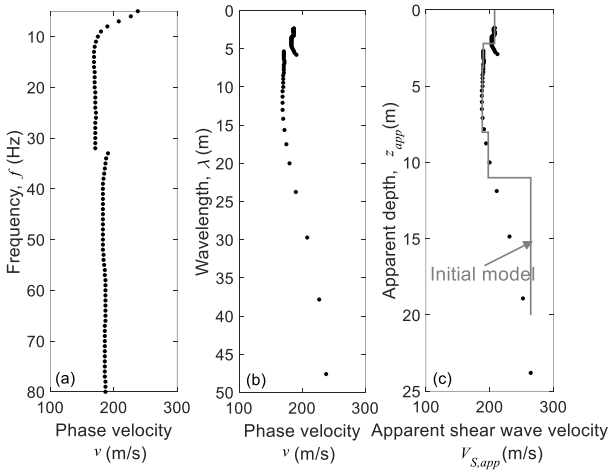

Figure 4. Initial model schematic: (a) Apparent dispersion curve in f-v domain; (b) Apparent dispersion curve in λ-v domain; (c) Apparent shear wave velocity profile where the gray line is the initial model.

3.2. Different inversion schemes

Three different inverted approaches are compared: **(1)** SASW effective mode (EM) inversion, **(2)** MASW fundamental mode (FM) inversion, and **(3)** MASW frequency-velocity spectrum (FVS) inversion.

SASW effective mode inversion attempts to fit individual experimental dispersion curves obtained from different receiver spacing with the theoretical dispersion curves, which is called the "effective" or "apparent" as it considers receiver locations and superposition of modes. The commercial software, WinSASW (Joh, 1996), is used as the tool for SASW inversion in the study including the signal processing to extract dispersion curves. The 3D array inversion approach in WinSASW is applied for SASW effective mode inversion.

MASW fundamental mode inversion assumes that the measured dispersion curve from multi-station signals represents the fundamental mode. The misfit objective

function (Φ_{FM}) for the MASW fundamental mode inversion is defined as

$$\Phi_{FM} = \sum_{f} \left(v_m(f) - v_{FM}(f) \right)^2 \tag{5}$$

where $v_m(f)$ is the picked fundamental mode dispersion curve from the measured FVS peaks; $v_{FM}(f)$ is the theoretical fundamental mode. It should be noted that $v_{FM}(f)$ is independent of source and receiver locations.

MASW frequency-velocity spectrum inversion infers the earth profile by directly fitting the measured frequency-velocity spectrum with the theoretically predicted one by the dynamic response solution:

$$\Phi_{FVS} = \sum_{v} \sum_{f} \frac{\left| \left| \hat{W}_m(f,v) \right| - \left| \hat{W}(f,v) \right| \right|}{\left| \hat{W}_m(f,v) \right|} \tag{6}$$

where $|\hat{W}_m(f,v)|$ is the measured frequency-velocity spectrum using field data in Eq. (4), and $|\hat{W}(f,v)|$ is the predicted frequency-velocity spectrum by substituting the time-harmonic solution in Eq. (2) as the measured data into Eq. (4).

A build-in local search algorithm (fminsearch.m) in MATLAB is used for finding the best fit in MASW fundamental mode and frequency-velocity spectrum inversion.

4. Comparison of different inversion schemes

4.1. Profile with mild V_S contrast

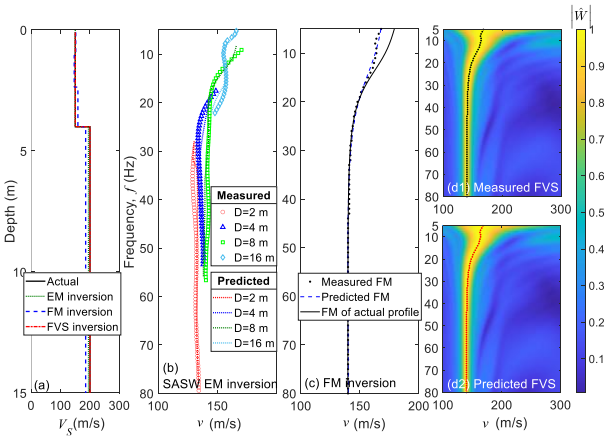

Figure 5. Inverted results for Model 1 by different inversion approaches: (a) inverted V_S profiles, and the fitting of (b) SASW effective mode (EM) dispersion curves, (c) MASW fundamental mode (FM) dispersion curve, and (d) MASW frequency-velocity spectrum (FVS).

The inverted results of Model 1 are shown in Fig. 5. Figure 5(b) shows the fitting of SASW effective dispersion curves, the predicted effective dispersion curves (dotted lines) fit the measured one (hollow symbols) quite well by WinSASW. The predicted fundamental mode dispersion curve is also in good agreement with the measured one as shown in Fig. 5(c). However, they both slightly deviate from the actual fundamental mode (dark solid line in Fig. 5(c)) at low frequencies due to wavefield truncation from nearest offset and receive spread used. The actual fundamental mode dispersion curve is known because the synthetic model that generates the data is given. Finally, the measured frequency-velocity spectrum and predicted one are shown in Fig. 5(d1) and Fig. 5(d2), respectively. All the inversion approaches work reasonably well, only the MASW fundamental mode inversion slightly underestimates deeper V_S. This is due to the error in estimating the fundamental mode dispersion curve.

4.2. Profile with high V_S contrast

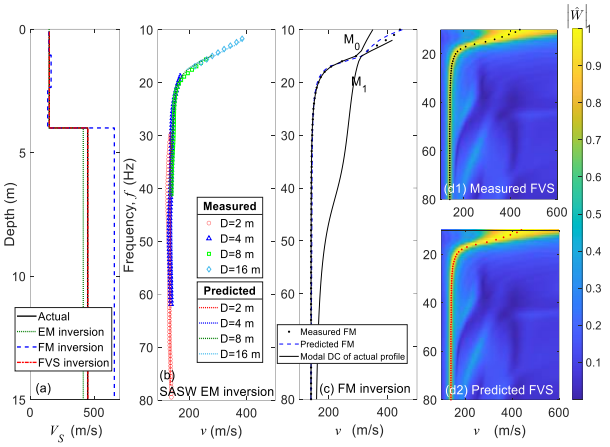

Figure 6. Inverted results for Model 2 by the three different inversion approaches: (a) inverted V_S profiles, and the fitting of (b) SASW effective mode (EM) dispersion curves, (c) MASW fundamental mode (FM) dispersion curve, and (d) MASW frequency-velocity spectrum (FVS).

A simple two-layer model with high V_S contrast (Model 2) is examined by the three different inversion approaches. In this kind of profile, the dispersion energy may be dominated by the first higher mode below a certain frequency, which can be extended to lower frequencies as a leaky mode (fast-guided waves) where there are no roots in the dispersion equation (Lin et al., 2023). Both the SASW effective mode inversion and MASW frequency-velocity spectrum inversion work quite well since they consider the actual dynamic response at receiver locations. On the other hand, MASW fundamental mode inversion significantly overestimates V_S in the lower half-space by more than 40% (Fig. 6(a)). In the case where the lower half-space has a significantly higher V_S than the overlain layers, lower-frequency fundamental mode is connected to the first higher mode and fast-guided leaky mode in the frequency-velocity spectrum, as shown in Fig. 6(c). The overestimation of deeper V_S is due to the misidentification of fundamental mode (Gao et al., 2014).

4.3. Profile with low-V_S half-space

In the case of Model 3 where the V_S of the underlying half-space is smaller than those of the upper layers, there is a large frequency range where roots for the dispersion equation (i.e., det[***K***]=0) do not exist (Lin et al., 2023). In this case, the FVS peaks correspond to local minima of det[***K***]. In practice, we use real(det[***K***])=0 as the approximation and denote the roots as FM*. In FM* inversion, we fit the measured dispersion curve with the theoretical FM*. On the other hand, SASW effective

mode inversion and MASW frequency-velocity spectrum inversion do not have this issue because the inversion kernel is the dynamic response, not the normal mode. Nevertheless, all three approaches yield reasonable inverted results, as shown in Fig. 7. Some errors can be observed in FM* inversion due to the discrepancies between the peaks in frequency-velocity spectrum and roots of real(det[$\boldsymbol{K}$])=0.

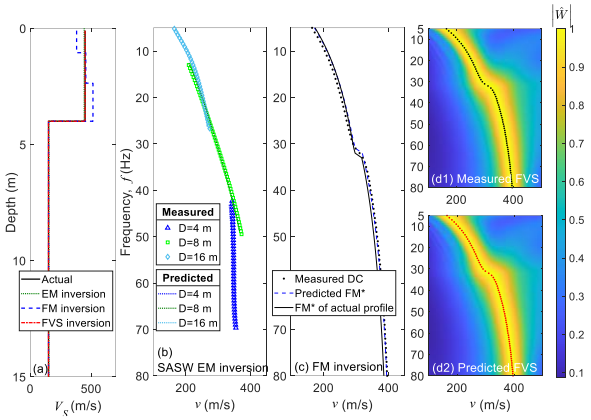

Figure 7. Inverted results for Model 3 by the three different inversion approaches: (a) inverted V_S profiles, and the fitting of (b) SASW effective mode (EM) dispersion curves, (c) MASW fundamental mode (FM) dispersion curve, and (d) MASW frequency-velocity spectrum (FVS).

4.4. Profile with embedded soft layer

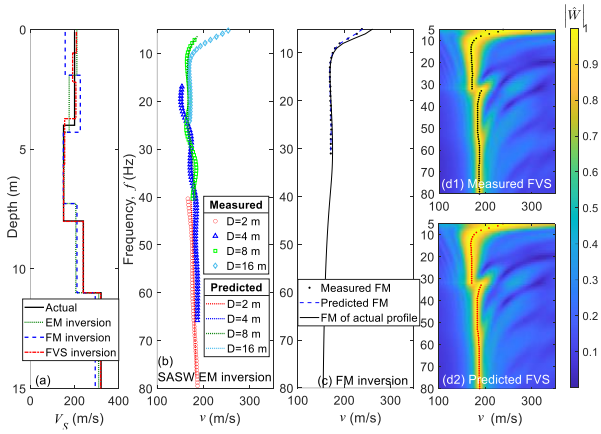

Figure 8. Inverted results for Model 4 by the three different inversion approaches: (a) inverted V_S profiles, and the fitting of (b) SASW effective mode (EM) dispersion curves, (c) MASW fundamental mode (FM) dispersion curve, and (d) MASW frequency-velocity spectrum (FVS).

In this scenario, the dominant mode jumps to higher modes when frequency increases (Fig. 8(d1)). The MASW fundamental mode inversion needs to discard the higher modes information at higher frequencies (smaller wavelengths) and extracts the fundamental mode. Therefore, the MASW fundamental mode inversion has a reasonable inverted profile, but it has poorer spatial resolution at shallow depths. Both the SASW effective mode inversion and the MASW frequency-velocity spectrum inversion include the higher mode information and perform well, while the frequency-velocity spectrum inversion has a better fit to the actual profile (Fig. 8(a)).

5. Field example

The synthetic examples demonstrate the good performance and robust automation of MASW frequency-velocity spectrum inversion in different scenarios of V_S profiles. A field example is further used to demonstrate the practical applications of MASW frequency-velocity spectrum inversion.

The field test was conducted at the courtyard of Min Ann Temple in Yuan Lin Township, Taiwan. Seismic waves were generated by a sledgehammer impacting on a circular steel plate and recorded by an array of 4.5 Hz vertical geophone. The receiver array is 23 m long with 1 m receiver spacing and 15 m nearest offset. The data was recorded with 0.5 ms sampling rate and 2048 samples. A P-S logging test was conducted in a borehole near the middle of the survey line, and it is taken as a benchmark of the inverted V_S profile. The same inversion procedure as described in Section 3.1 is performed, except that the z_{max} is a variable that needs to be adjusted to better fit the data. Figure 9 shows the measured frequency-velocity spectrum and its inverted V_S profile. The measured frequency-velocity spectrum (Fig. 9(b)) shows dominant higher modes at higher frequencies, indicating there is an embedded soft layer similar to Model 4. The predicted frequency-velocity spectrum (Fig. 8(c)) matches the measured frequency-velocity spectrum (Fig. 8(b)) extremely well, and the inverted V_S profile agrees with the results measured by the P-S logging.

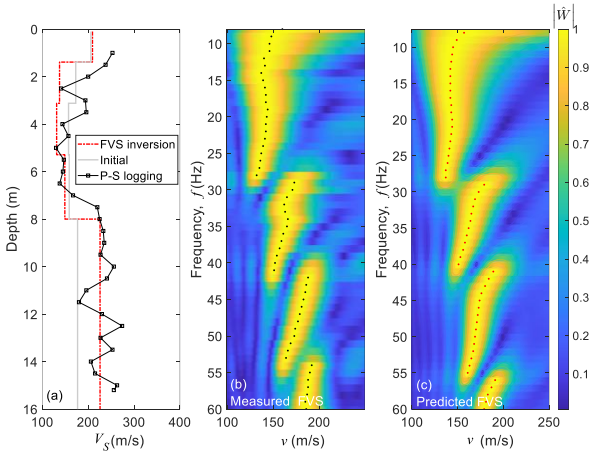

Figure 9. Results of MASW frequency-velocity spectrum inversion for the field example: (a) inverted V_S profile in comparison with the results of P-S logging; (b) the observed frequency-velocity spectrum (FVS); (c) the theoretical frequency-velocity spectrum of the inverted profile. The dots in (b) and (c) are the spectral peaks.

6. Conclusions

The MASW frequency-velocity spectrum inversion combines the convenience and robustness of MASW dispersion analysis with the rigorous inversion scheme of SASW, which is based on the actual dynamic response at receiver locations and considers possible higher modes and non-Rayleigh waves. Four different V_S profiles are used to compare the inverted results among the three different inversion approaches: SASW effective mode inversion, MASW fundamental mode inversion, and the proposed MASW frequency-velocity spectrum inversion. Fundamental mode inversion may obtain the incorrect V_S

estimation due to misidentification of mode(s) and truncation effect. The results of SASW effective mode inversion and MASW frequency-velocity spectrum inversion are theoretically similar and can produce better inverted results than the MASW fundamental mode inversion. However, the process of MASW frequency-velocity spectrum inversion is more convenient and robust. A field example, in which the frequency-velocity spectrum shows dominant higher modes at higher frequencies due to embedded soft layer, is used to show the practicality and advantages of frequency-velocity spectrum inversion. Further studies can be carried out to improve the model parameterization and the inversion algorithm based on frequency-velocity spectrum.

Acknowledgements

The authors are grateful for the financial support provided by the National Science and Technology Council, Taiwan, R. O. C. through the project 110-2625-M-A49.

References

Dou, S., and Ajo-Franklin, J. B. 2014. "Full-wavefield inversion of surface waves for mapping embedded low-velocity zones in permafrost." Geophysics, 79(6): EN107–EN124. https://doi.org/10.1190/geo2013-0427.1

Forbriger, T. 2003. "Inversion of shallow-seismic wavefields: II. Inferring subsurface properties from wavefield transforms." Geophys J Int, 153(3): 735–752. https://doi.org/10.1046/j.1365-246X.2003.01985.x

Gao, L., Xia, J., and Pan, Y. 2014. "Misidentification caused by leaky surface wave in high-frequency surface wave method." Geophys J Int, 199(3), 1452–1462. https://doi.org/10.1093/gji/ggu337

Gabriels, P., Snieder, R., and Nolet, G. 1987. "In situ measurements of shear-wave velocity in sediments with higher mode Rayleigh waves." Geophys Prospect, 35(2): 187–196. https://doi.org/10.1111/j.1365-2478.1987.tb00812.x

Joh, S. H. 1996. "Advances in the data interpretation technique for Spectral-Analysis-of-Surface-Waves (SASW) measurements." PhD thesis, University of Texas at Austin, TX, USA.

Kausel, E., and Roësset, J. M. 1981. "Stiffness matrices for layered soils." Bull Seismol Soc Am, 71(6), 1743–1761. https://doi.org/10.1785/BSSA0710061743

Lin, C. P., Pan, E., Tran, Q. K., and Wu, T. J. 2023. "A unified approach for relationships among Green's function, normal modes and dispersion spectrum in layered elastic half-space, with corrected misconceptions on surface wave dispersion and testing." Geophys J Int, 232(2), 1357–1375. https://doi.org/10.1093/gji/ggac396

Lin, C. P., Wu, T. J., and Pan, E. 2022. "An efficient full-wavefield computational approach for seismic testing in a layered half-space." Soil Dyn Earthq Eng, 161, 107423. https://doi.org/10.1016/j.soildyn.2022.107423

Park, C. B., Miller, R. D., and Xia, J. 1998. "Imaging dispersion curves of surface waves on multichannel record." In: *68th Annual International Meeting*, 1377–1380. New Orleans, Louisiana: Society of Exploration Geophysicists. https://doi.org/10.1190/1.1820161

Park, C. B., Miller, R. D., and Xia, J. 1999. "Multichannel analysis of surface waves." Geophysics, 64(3), 800–808. https://doi.org/10.1190/1.1444590

Pelekis, P. C., and Athanasopoulos, G. A. 2011. "An overview of surface wave methods and a reliability study of a simplified inversion technique." Soil Dyn Earthq Eng, 31(12), 1654–1668. https://doi.org/10.1016/j.soildyn.2011.06.012

Ryden, N., and Park, C. B. 2006. "Fast simulated annealing inversion of surface waves on pavement using phase velocity spectra." Geophysics, 71(4), R49–R58. https://doi.org/10.1190/1.2204964

Stokoe II, K. H., Wright, S. G., Bay, J., and Roesset, J. M. (1994). "Characterization of geotechnical sites by SASW method." In *Geophysical characterization of sites, ISSMFE Technical Committee #10*, edited by R. D. Woods, 15–25. Oxford Publishers, New Delhi.